Journal of Alloys and Compounds 509 (2011) 3019–3024

Contents lists available at ScienceDirect

Journal of Alloys and Compounds

journal homepage: www.elsevier.com/locate/jallcom

Deposition and characterization of $CuInSe_2$ films for solar cells using an optimized chemical route

M. Berruet[a], W.H. Schreiner[b], S. Ceré[a], M. Vázquez[a,*]

[a] División Corrosión, INTEMA, CONICET, Facultad de Ingeniería, Universidad Nacional de Mar del Plata, Juan B. Justo 4302, B7608FDQ Mar del Plata, Argentina
[b] Laboratório de Superfícies e Interfases, Departamento de Física, Universidade Federal do Paraná, 81531-990 Curitiba, PR, Brazil

ARTICLE INFO

Article history:
Received 22 September 2010
Received in revised form 3 November 2010
Accepted 18 November 2010
Available online 19 December 2010

Keywords:
Thin films
Semiconductors
Chemical synthesis

ABSTRACT

$CuInSe_2$ (CISe) thin films have been deposited on glass using successive ionic layer adsorption and reaction (SILAR). The as-deposited films are treated at 400 °C in argon atmosphere and etched in KCN solution to remove detrimental secondary phases. The preparation and temperature of the precursor solutions, the duration of the reaction cycles and the duration of the annealing stage have been optimized. The films have been characterized employing grazing incident X-ray diffraction, Raman spectroscopy, X-ray photoelectron spectroscopy, scanning electron microscopy and energy dispersive scanning spectroscopy. Relevant semiconductor parameters have been calculated. Photoelectrochemical tests confirm p-type conduction. The films are crystalline and the stoichiometry can be improved by renewing the precursor solution after completing half of the cycles, annealing for 90 min and later etching in KCN. The quality of the material seems to be promising for application in solar cell devices.

1. Introduction

Copper indium selenides are typical chalcogenides characterized by their high absorption coefficient and a band gap energy value close to that of the solar radiation. For these reasons, these materials are frequently chosen for photovoltaic applications.

Recent advances have been achieved in the production of chalcogenides for thin film solar cells using techniques based in reactive pulses, like atomic layer deposition (ALD) or chemical vapour deposition (CVD) [1–3] and pulsed electrodeposition [4]. With these methods, the key components are delivered onto the substrate in gaseous reactive cycles. Despite this, the main disadvantages are the low deposition rate and the high production costs, which complicate scaling these processes to large production of solar cells.

Successive ionic layer adsorption and reaction (SILAR) constitutes a recently introduced chemical method, suitable for the deposition of thin films [5]. The method is based on sequential heterogeneous reactions between the solid phase and the solvated ions in the solution, which take place directly on the desired substrate surface. The most interesting features of this method include excellent material utilization efficiency without requiring high vacuum (cost-effectiveness), the possibility of controlling the film thickness and large-scale deposition capability on many types of different substrates [6,7].

When using the SILAR method, the purity, composition, temperature and pH values of the precursor solutions together with reaction time are among the main parameters that influence the film growth [8–11]. Besides, finding residual, unreacted, binary phases, such a $CuSe_x$, is a well-known disadvantage, usually solved by etching with a solution of KCN [12].

This investigation aims at optimizing the variables that govern the process, so as to enhance crystallinity and improve the composition of the films. While adjusting the experimental settings, the crystallographic, compositional, optical and morphological properties of $CuInSe_2$ have been extensively studied. In particular, the precursor solutions have been renewed after completing half of the cycles. Also, the duration of the thermal treatment has been increased. Both factors seem to have contributed to improve the overall quality of the films in terms of composition and stoichiometry.

Future research will focus on the use of SILAR to infiltrate nanoporous oxides and to prepare solar cells.

2. Experimental details

2.1. Substrate and precursor solutions

Glass coated with a transparent conducting oxide (TCO, SnO_2:F, Libbey Owens Ford, TEC 8/3 mm) and uncoated glass are used as substrates. Prior to use, the substrates are degreased with detergent solution followed by rinsing in an ultrasonic bath with ethanol and acetone for 10 min respectively.

* Corresponding author. Tel.: +54 223 481 6600; fax: +54 223 481 0046.
E-mail address: mvazquez@fi.mdp.edu.ar (M. Vázquez).

0925-8388/$ – see front matter © 2010 Elsevier B.V. All rights reserved.
doi:10.1016/j.jallcom.2010.11.190

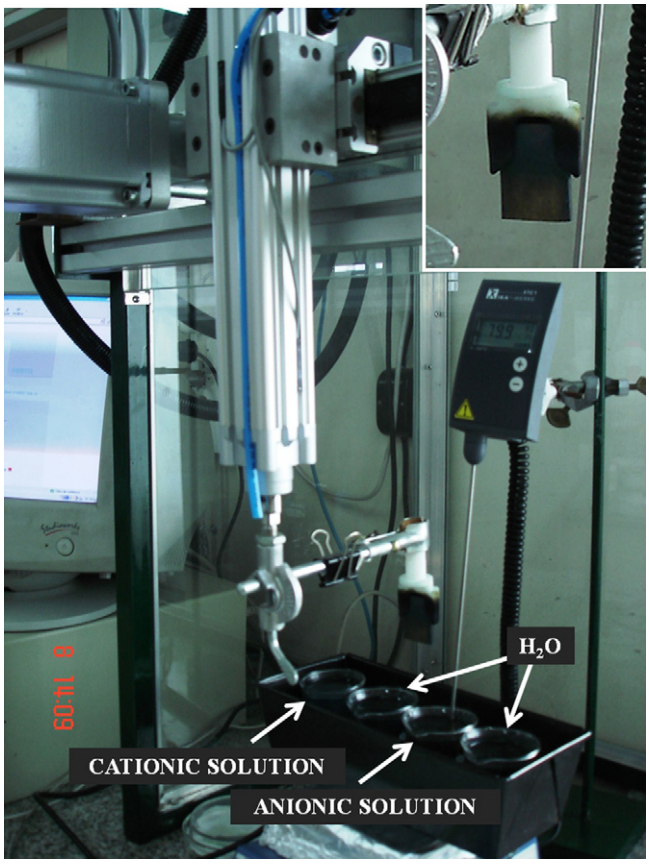

Fig. 1. Customized set-up for the implementation of the SILAR method. The inset shows the sample holder in greater detail.

The solutions are prepared using AR grade chemicals and referred to as cationic and anionic precursor solutions respectively. The cationic precursor solution is prepared from two separated solutions, one containing 0.06 mol L^{-1} indium chloride ($InCl_3$) complexed with 0.06 mol L^{-1} sodium citrate (CitNa) and the other 0.06 mol L^{-1} cupric chloride ($CuCl_2$) complexed with 0.6 mol L^{-1} triethanolamine (TEA) respectively. These are then mixed, stirring continuously for 1 h. The anionic precursor solution is prepared by refluxing and stirring continuously 0.025 mol Se and 0.05 mol Na_2SO_3 in 0.25 L deionized water at 100 °C for 2 h, where reactions (I) and (II) take place [11]:

$$Se + Na_2SO_3 \rightarrow Na_2SeSO_3 \quad (I)$$

$$SeSO_3^{2-} + 2OH^- \rightarrow Se^{2-} + SO_4^{2-} + H_2O \quad (II)$$

After cooling to room temperature, the unreacted selenium is filtered off and the selenosulfate solution (effective concentration = 0.1 mol L^{-1}) is stored in a dark bottle and used within 48 h. Then, when used, this solution is diluted to reach a final concentration of 0.06 mol L^{-1}. The pH value of the cationic precursors is adjusted to 8, while the pH value of the anionic precursors is fixed at 8.5.

2.2. SILAR deposition

$CuInSe_2$ films are deposited at 80 °C by alternative immersion in the two solutions containing the cationic and anionic precursors. The deposition system is assembled with a mechanical arm operated by customized software (Fig. 1). Each dipping cycle consists of the following sequence: (a) the clean substrate is immersed into the cationic precursor solution for t_p seconds, and then rinsed with deionized water for t_r seconds to remove the unattached ions at the same temperature; (b) the substrate is immersed into the anionic precursor solution for t_p seconds and rinsed with water for t_r seconds. Each cycle is repeated 75 times. Two different alternatives were evaluated. In set-up #1 (S1) the 75 cycles are repeated with t_p = 30 s and t_s = 10 s. In set-up #2 (S2), after completing the first 40 cycles, the deposition is interrupted and the solutions are renewed to prevent contamination and a decrease in the concentration of precursors. After the renewal, 35 more cycles are repeated. In this case, t_p = 35 s and t_s = 20 s.

During each cycle, the Cu^{2+} and In^{3+} adsorbed ions on substrate react to form binary compounds, CuSe and In_2Se_3, as described by reactions (III) and (IV) [11]:

$$Cu(TEA)^{2+} + Se^{2-} \rightarrow CuSe + TEA \quad (III)$$

$$2(In\text{-}CitNa)^{3+} + 3Se^{2-} \rightarrow In_2Se_3 + 2CitNa \quad (IV)$$

Finally, the films are annealed at 400 °C in argon atmosphere for 60 min for S1 and 90 min for S2, where $CuInSe_2$ is formed, as described by reaction (V):

$$2CuSe + In_2Se_3 \rightarrow 2CuInSe_2 + Se \quad (V)$$

After annealing, some samples are chemically etched in 0.5–1 mol L^{-1} KCN to remove secondary phases [12,13].

2.3. Characterization

The films are analyzed by X-ray diffraction using a PANalytical X'Pert Pro diffractometer, Cu-Kα radiation at 40 kV and 40 mA. The samples are scanned between 20° and 80° with a speed of 0.02°/s and grazing incidence. The crystallographic data for each phase are taken from the literature and analyzed with X'Pert HighScore software.

Raman spectra are performed using an Invia Reflex confocal Raman microprobe. Excitation is provided with the 514 nm emission line of an Ar+ laser and measurements are performed in backscattering configuration using a 50× objective.

X-ray photoelectron spectroscopy (XPS) spectra are taken using a commercial VG Microtech ESCA 3000 system. The spectra are collected using Al-Kα radiation. Survey spectra are recorded for the samples in the 0–1100 eV binding energy range by 1 eV steps and a bandpass of 50 eV (not shown). High resolution scans with 0.1 eV steps and bandpass of 20 eV are conducted over the following regions of interest: In 3d, O 1s, Se 3d, Cu 2p. In every case, surface charging effects are compensated by referencing the binding energy (BE) to the C 1s line of residual carbon set at 284.5 eV BE [14]. Spectral decomposition assumed mixed Gaussian–Lorenzian curves and is performed by using Shirley background subtraction and a least square fitting program.

The morphology of the layers is studied with scanning electron microscopy (SEM), using a JEOL JSM-6460LV microscope. The composition is analyzed by X-ray energy dispersive spectroscopy (EDS). The system used is an EDAX Genesis XM4 – Sys 60, equipped with Multichannel Analyzer EDAX mod EDAM IV, Sapphire Si(Li) detector and Super Ultra Thin Window of Be, and EDAX Genesis software.

The band gap energy can be calculated from the absorption spectra registered using a double beam UV/vis Shimadzu UV-160A.

All the photoelectrochemical (PEC) characterizations are carried out in a standard three-electrode cell together with a Pt mesh as counter electrode and a saturated calomel electrode (SCE) as reference and monitored by an IVIUM Compact potentiostat. The experiments were performed at room temperature and the solutions were bubbled with nitrogen for 30 min before use. The working electrode area is 1.41 cm^2. The light source is a 150 W Xe lamp coupled with a 380 nm UV-filter. The light intensity is evaluated using a Si-photodiode. Photocurrent and photopotential are evaluated forming a semiconductor/electrolyte junction by immersion of the TCO/CISe film in a 0.2 mol L^{-1} KCl solution. The light is chopped using an electronic shutter (Uniblitz® model T132).

3. Results and discussion

Fig. 2 presents a comparison of GXRD diffractograms from as-deposited, annealed and etched samples prepared with set-up S2. The most characteristic peaks of the chalcogenide structure

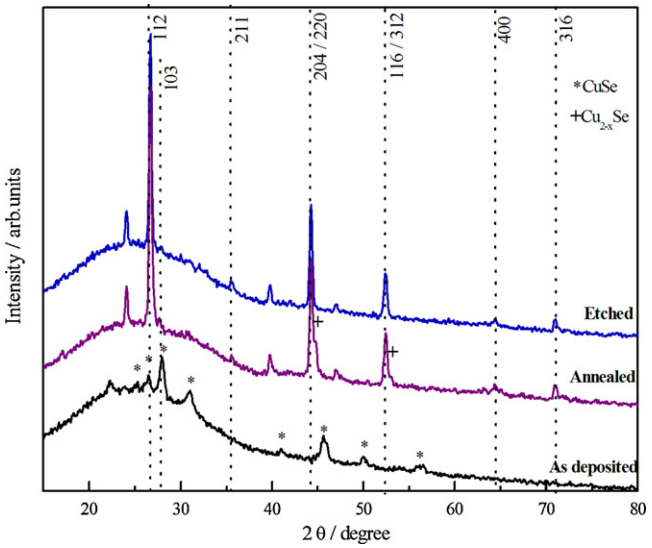

Fig. 2. Typical GXRD diffractograms of CISe thin films on glass. As-deposited, annealed and etched samples prepared with set-up S2 are compared.

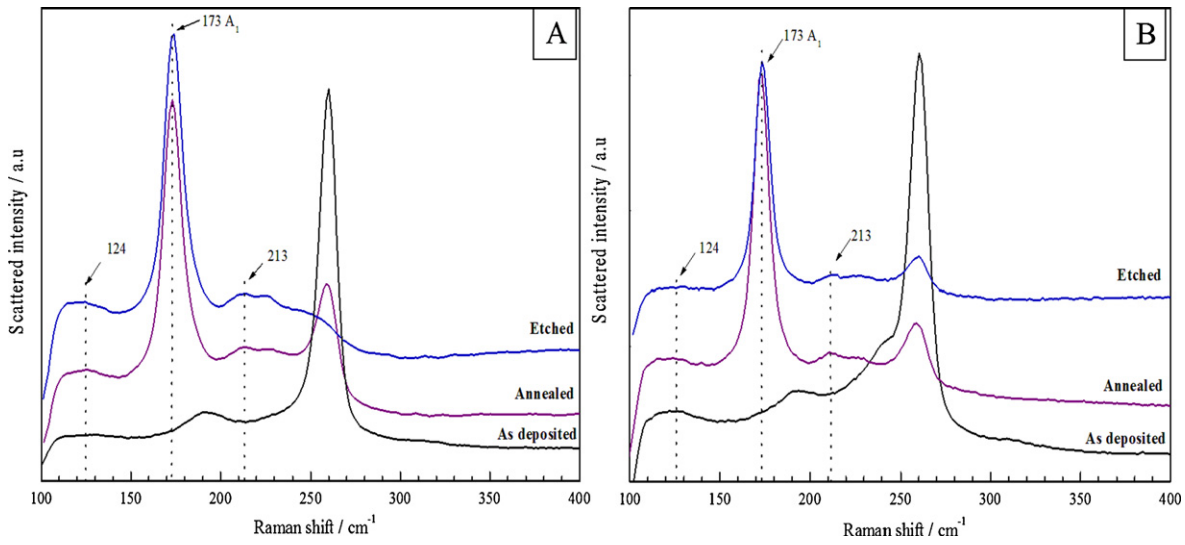

Fig. 3. Typical Raman spectra of CISe thin films prepared with: (a) set-up S2; (b) set-up S1. As-deposited, annealed and etched samples are compared.

are present in the annealed and etched samples such as (1 1 2), (2 2 0/2 0 4), (1 1 6/3 1 2). The peaks of $CuInSe_2$ are narrow, intense and maintain the same relative intensity than those in JCPDS cards (no. 40-1487). As expected, the conversion of the mostly amorphous binary compounds into crystalline CISe takes place during the thermal treatment. Later, the etching stage with KCN solution greatly contributes in eliminating residual binaries.

The Raman spectra shown in Fig. 3 confirm the results discussed above. The as-deposited film prepared with set-up S2 (Fig. 3a) presents a very intense peak at 258 cm^{-1} that can be attributed to the formation of Cu_xSe and ill-defined peaks at 196 cm^{-1} and 240 cm^{-1} which can be ascribed to vibration modes of Cu_3Se_2 and Se respectively [15,16]. The annealed sample presents the A_1 mode peak at 173 cm^{-1} related to the vibration of Se–Se bonds (anions) and weak peaks at 124 cm^{-1} and 213 cm^{-1} typical of the Cu–In bonds (cations)[17]. The peak at 258 cm^{-1} reveals the presence of residual Cu_xSe. Once again, etching in KCN successfully removes this undesired binary compound, so that all the peaks in the spectrum of the etched sample correspond to $CuInSe_2$, which is in agreement with GXRD results. Fig. 3b shows Raman spectra for $CuInSe_2$ samples prepared with set-up S1. In this case, the peaks at 124 cm^{-1} and 213 cm^{-1} typical of the Cu–In bonds are not as evident as in Fig. 3a, even after annealing and etching the sample. Also, residual Cu_xSe cannot be completely eliminated by KCN etching.

The oxidation states of the elements in the synthesized $CuInSe_2$ were further explored by XPS. Fig. 4a shows the Cu 2p core level spectrum. The peak at 932.3 eV corresponding to the $Cu2p_{3/2}$ is in good agreement with the reported values for Cu^+ [18]. It is worth noting that the satellite peak corresponding to the binding energy of Cu^{2+} usually located at 942 eV is not observed in the XPS spectrum [19]. Fig. 4b shows the In 3d core level spectrum. The observed peaks, centered at 444.7 eV and 452.9 eV, correspond to In $3d_{5/2}$ and In $3d_{3/2}$ respectively. The selenium 3d core level is shown in Fig. 4c. The main peak at 53.4 eV corresponds to the Se $3d_{5/2}$, as reported earlier for the $CuInSe_2$ [20] and the peak at 54.95 eV is attributed to Se^0.

The elemental composition of the film in atomic percentage can be determined by energy dispersive spectroscopy (EDS) as shown in Table 1, where as-deposited, annealed and etched samples are compared. As can be seen, it is during the annealing stage that the stoichiometry of the CISe layer is consolidated. A noticeable improvement is produced using set-up S2. In this case, the precursor solutions are renewed after completing half of the cycles and more time is given to the rinsing stage. Also, the duration of the thermal treatment is increased. The first two factors aim at keeping

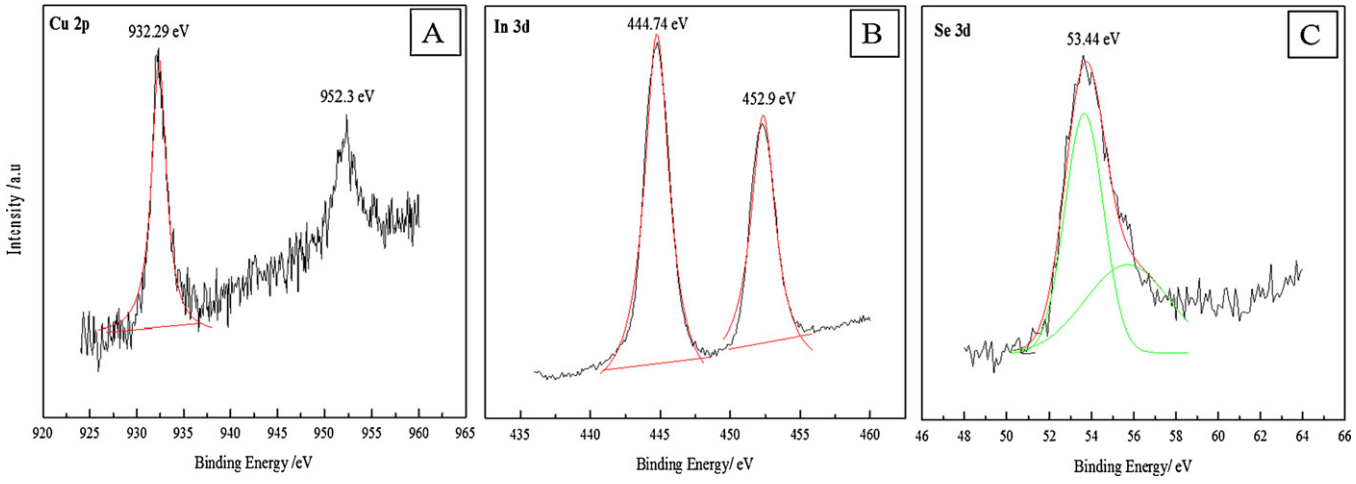

Fig. 4. XPS spectra of $CuInSe_2$ film prepared with set-up S2. (a) Cu $2p_{3/2}$; (b) In $3d_{5/2}$ and (c) Se $3d_{5/2}$ regions.

Table 1
Elemental composition of the film in atomic percentage.

Thin films	Atomic relation			
	Cu/Se	In/Se	Cu/In	Se/(Cu + In)
Stoichiometric $CuInSe_2$	0.5	0.5	≤1	1
Set-up S1				
As deposited	0.63	0.08	8.14	1.4
Annealed	0.66	0.49	1.35	0.88
Etched	0.46	0.71	0.65	0.85
Set-up S2				
As deposited	0.63	0.13	5	1.3
Annealed	2.48	1.06	2.33	0.28
Etched	0.53	0.53	1	0.94

the concentration of the reactants more constant, while reducing the incidence of cross contamination between the anionic and cationic solutions. Also, by extending the duration of the annealing stage a better conversion from reactants into products was achieved. All of them contributed to improve the overall quality of the films in terms of composition and stoichiometry. Finally, etching with KCN is a key step. When annealed CISe films are etched, no detachment of the film can be seen.

Fig. 5 presents SEM photographs of the films deposited on TCO for annealed and etched samples. Both variations of the experimental set-up show a good coverage. The morphology of the CISe obtained with set-up S1 is in good agreement with that reported by other authors [8,9,21]. When using set-up S2, the morphology is different, tending to form platelets. This change goes along with the improvement in composition detected by EDS, and is likely due to the same factors that were discussed above. Fig. 5e shows a cross-section of an annealed film deposited on TCO. As the film is partially detached, the thickness can be estimated to be 1.5 μm, as expected from the estimation published by Yang et al. [9], taking into account the number of cycles and the temperature used in the preparation of this sample.

The absorption coefficient (α) and the band gap energy (E_g) can calculated from UV–vis absorption spectra. The optical density (OD) can be defined as:

$$\mathrm{OD} = -\log\left(\frac{I(l)}{I_o}\right) \quad (1)$$

where $I(l)$ is the radiation absorbed by the CISe film and I_o is that absorbed by the substrate. The absorption coefficient α is given by the relationship between the optical density and the thickness of

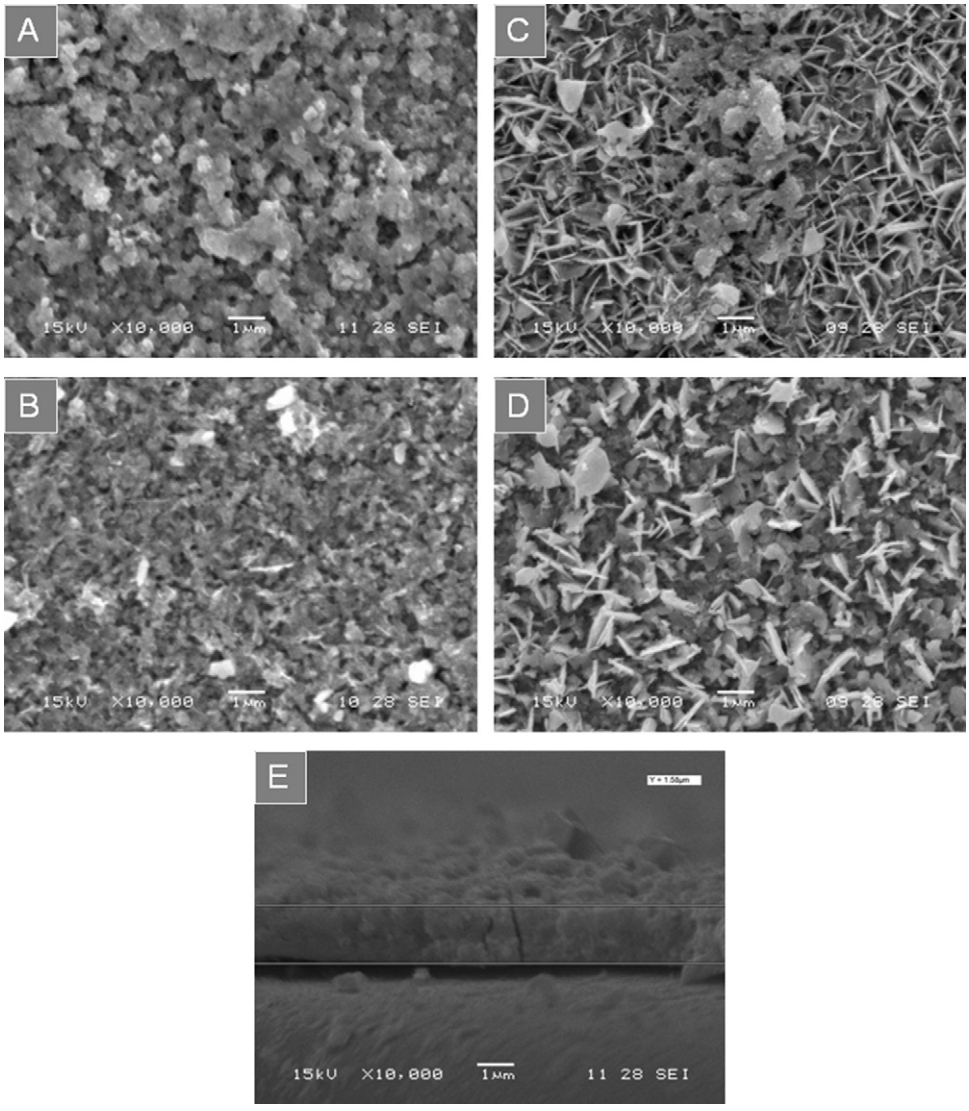

Fig. 5. SEM pictures of $CuInSe_2$ deposited on TCO. (a) Prepared with S1; (b) prepared with S1 and etched in KCN solution; (c) prepared with S2; d) prepared with S2 and etched in KCN solution; e) Cross sectional view of an annealed CISe film prepared with S2.

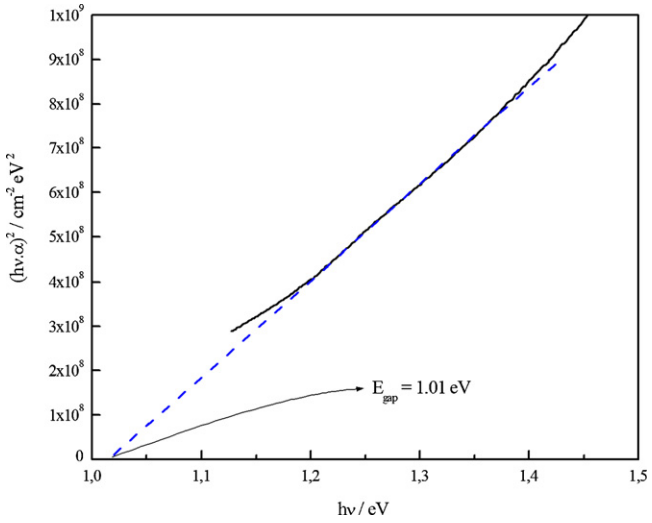

Fig. 6. E_g determination for $CuInSe_2$ prepared with S2 on glass.

the absorbing medium (d), which is taken as 1 μm (after etching).

$$\alpha = \frac{\mathrm{OD}}{0.434d} \tag{2}$$

The expected variation from the absorption coefficient (α) with the photon energy for a direct band gap semiconductor is given by:

$$\alpha = \frac{c(h\upsilon - E_g)^{1/2}}{h\upsilon} \tag{3}$$

where c is a constant. From Eq. (3), E_g can be calculated from absorption spectra by plotting $(\alpha h\nu)^2$ versus $(h\nu)$, as shown in Fig. 6. The calculated E_g results equal to 1.01 eV, in good agreement with values previously reported in the literature for CISe prepared by techniques such as electrodeposition, ALD and CVD, among others [22–24].

It is well known that the semi conducting properties of chalcopyrites depend on the non-stoichiometry and are governed by the presence of intrinsic defects such as vacancies and interstitials [21]. Furthermore, the predominant type of conduction can be either n- or p-type depending on preparation methods. Photoelectrochemistry can be used to elucidate the nature of the carriers. The main effect of periodic illumination on the current driven by semiconductor electrodes under potentiostatic control is the creation of electron–hole pairs, which alters the concentration of minority carriers and thereby promotes processes governed by minority carrier concentration. During photoexcitation, both photopotential and photocurrent can be observed. The photoexcited electrons and holes are separated in the space charge layer, with each moving in opposite directions across the electric field. This migration induces an inverse potential in the electrode (photopotential) which reduces the potential difference across the space charge layer and retards the migration of the carriers. In the case of p-type semiconductors, the Fermi level of the semiconductor interior decreases (the electrode potential increases) when the band edge level bends downward in the space charge layer. Moreover, photocurrent is registered when the electrons photoproduced in the space charge region move towards the electrode/electrolyte interface and increase the cathodic current. Fig. 7 shows the photopotential and the photocurrent registered at open circuit potential. With illumination, the potential moves to more positive values (positive photopotential) and the current moves in the negative direction (negative photocurrent), confirming the p-type nature of the film.

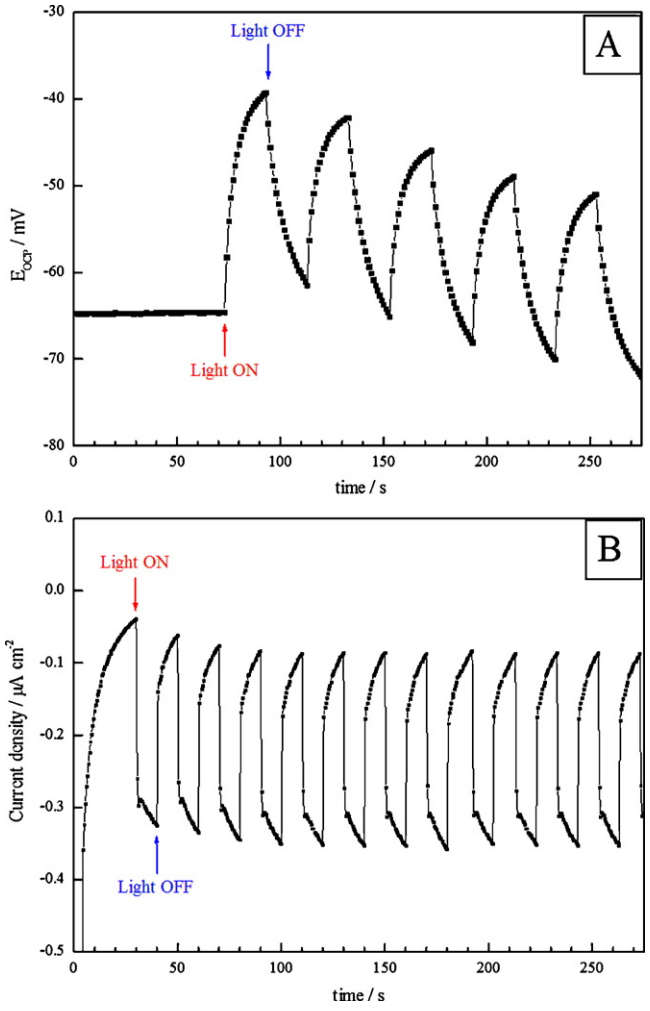

Fig. 7. Evolution of (a) photopotential and (b) photocurrent in time, registered at open circuit potential in a 0.2 mol L^{-1} KCl solution.

4. Conclusions

$CuInSe_2$ (CISe) has been obtained by SILAR, showing absorption, XRD, XPS and Raman spectra in good agreement with those reported for the crystalline material obtained by conventional methods.

The quality of the material seems to be promising for application in solar cell devices. Annealing in argon atmosphere proved to be essential to synthesize a crystalline material, while etching in KCN solution guarantees the removal of secondary phases that are detrimental for the electronic properties of the film. Renewing the precursor solutions after completing half of the cycles, increasing the rinsing time and using longer thermal treatments, proved to improve the overall quality of the films in terms of composition and stoichiometry.

Photoelectrochemical tests confirm p-type conduction. The band gap energy can be calculated from absorption spectra, producing a value in good agreement with results published for CISe prepared by other methods.

The SILAR method can be useful when preparing large area, porous and nanograined electrodes for PEC cells at the expense of small amount of initial ingredients. Taking into account that the cyclic nature of this type of deposition methods may ease the infiltration of nanoporous structures or templates, the preparation of 3D CISe-based photovoltaic solar cells is currently in progress.

Acknowledgements

Support from YPF Foundation, Consejo Nacional de Investigaciones Científicas y Técnicas, Agencia Nacional de Promoción Científica y Tecnológica and Universidad Nacional de Mar del Plata from Argentina is acknowledged. We are grateful also to Mr. Sebastián Rodriguez and Dr. Sergio Pellice for their help during SILAR implementation.

References

[1] M. Leskelä, M. Ritala, Thin Solid Films 409 (2002) 138–146.
[2] N.N. Mishack, E.E. Chinedu, Chalcogenide Letters 7 (2010) 31–38.
[3] M. Nanu, J. Schoonman, A. Goossens, Advanced Materials 16 (2004) 453–456.
[4] F. Kang, J. Ao, G. Sun, Q. He, Y. Sun, Journal of Alloys and Compounds 478 (2009) L25–L27.
[5] H.M. Pathan, C.D. Lokhande, D.P. Amalnerkar, T. Seth, Applied Surface Science 211 (2003) 48–56.
[6] S.M. Pawar, B.S. Pawar, J.H. Kim, O.-S. Joo, C.D. Lokhande, Current Applied Physics (2010), doi:10.1016/j.cap.2010.07.007.
[7] H.M. Pathan, C.D. Lokhande, Bulletin of Materials Science 27 (2004) 85–111.
[8] Y. Shi, Z. Jin, C. Li, H. An, J. Qiu, Thin Solid Films 515 (2007) 3339–3343.
[9] J. Yang, Z. Jin, Y. Chai, H. Du, T. Liu, T. Wang, Thin Solid Films 517 (2009) 6617–6622.
[10] J. Yang, Z. Jin, C. Li, T. Wang, T. Liu, Materials Letters 62 (2008) 4177–4180.
[11] J. Yang, Z. Jin, T. Liu, C. Li, Y. Shi, Solar Energy Materials and Solar Cells 92 (2008) 621–627.
[12] P. Fons, S. Niki, A. Yamada, M. Nishitani, T. Wada, T. Kurafuji, Materials Research Society Symposium 426 (1996) 213–218.
[13] C. Guillen, J. Herrero, Solar Energy Materials and Solar Cells 43 (1996) 47–57.
[14] F. Moulder, W.F. Stickle, P.E. Sobol, K.D. Bomben (Eds.), Handbook of X-Ray Photoelectron Spectroscopy, Physical Electronics, Inc., Eden Praire, Minnesota 55344, USA, 1995.
[15] O. Ramdani, J.F. Guillemoles, D. Lincot, P.P. Grand, E. Chassaing, O. Kerrec, E. Rzepka, Thin Solid Films 515 (2007) 5909–5912.
[16] V. Izquierdo-Roca, X. Fontané, J. Álvarez-García, L. Calvo-Barrio, A. Pérez-Rodríguez, J.R. Morante, J.S. Jaime-Ferrer, E. Saucedo, P.P. Grand, V. Bermúdez, Thin Solid Films 517 (2009) 2163–2166.
[17] E.P. Zaretskaya, V.F. Gremenok, V. Riede, W. Schmitz, K. Bente, V.B. Zalesski, O.V. Ermakov, Journal of Physics and Chemistry of Solids 64 (2003) 1989–1993.
[18] C.R. Kim, S.Y. Han, C.H. Chang, T.J. Lee, S.O. Ryu, Current Applied Physics 10 (2010) S383–S386.
[19] H. Chen, S.-M. Yu, D.-W. Shin, J.-B. Yoo, Nanoscale Research Letters 5 (2010) 217–223.
[20] K. Bindu, C.S. Kartha, K.P. Vijayakumar, T. Abe, Y. Kashiwaba, Solar Energy Materials and Solar Cells 79 (2003) 67–79.
[21] M. Dhanam, B. Kavitha, S. Velumani, Materials Science and Engineering B 174 (2010) 209–215.
[22] J.M. Wrobel, J.J. Dubowski, The International Society for Optical Engineering 2703 (1996) 514–525.
[23] P.P. Hankare, K.C. Rathod, P.A. Chate, A.V. Jadhav, I.S. Mulla, Journal of Alloys and Compounds 500 (2010) 78–81.
[24] M. Valdés, M. Vázquez, A. Goossens, Electrochimica Acta 54 (2008) 524–529.